

Long-term persistence and multifractality of river runoff records: Detrended fluctuation studies

Eva Koscielny-Bunde^{1,2}, Jan W. Kantelhardt^{1,3}, Peter Braun⁴, Armin Bunde¹, and Shlomo Havlin^{5,1}

¹ Institut für Theoretische Physik III, Justus-Liebig-Universität, D-35392 Giessen, Germany.

² Potsdam Institute for Climate Impact Research, P. O. Box 60 12 03, D-14412 Potsdam, Germany.

³ Center for Polymer Studies and Department of Physics, Boston University, Boston MA 02215, USA.

⁴ Bayerisches Landesamt für Wasserwirtschaft, Lazarettstr. 67, D-80636 München, Germany.

⁵ Department of Physics and Minerva Center, Bar-Ilan University, Ramat-Gan 52900, Israel.

(submitted: March 6, 2003)

We study temporal correlations and multifractal properties of long river discharge records from 41 hydrological stations around the globe. To detect long-term correlations and multifractal behaviour in the presence of trends, we apply several recently developed methods [detrended fluctuation analysis (DFA), wavelet analysis, and multifractal DFA] that can systematically detect and overcome nonstationarities in the data at all time scales. We find that above some crossover time that usually is several months, the daily runoffs are long-term correlated, being characterized by a correlation function $C(s)$ that decays as $C(s) \sim s^{-\gamma}$. The exponent γ varies from river to river in a wide range between 0.1 and 0.9. The power-law decay of $C(s)$ corresponds to a power-law increase of the corresponding fluctuation function $F_2(s) \sim s^H$ where $H = 1 - \gamma/2$. Below the crossover time, the daily runoffs show a very different behaviour: They are nonstationary and characterized by H values being close to 1.5, similar to Brownian noise. We also study the multifractal properties of the records. We find that in all records, above several months, weak multifractality occurs. For all cases, the Renyi exponent $\tau(q)$ for q between -10 and $+10$ can be fitted to the remarkably simple form $\tau(q) = -\ln(a^q + b^q)/\ln 2$, with solely two parameters a and b between 0 and 1 with $a + b \geq 1$. This type of multifractality is obtained from a generalization of the binomial multifractal model.

I. INTRODUCTION

The analysis of river flows has a long history. Already more than half a century ago Hurst found by means of his R/S analysis that annual runoff records from various rivers (including the Nile river) exhibit "long-range statistical dependencies" [Hurst, 1951], indicating that the fluctuations in water storage and runoff processes are self-similar over a wide range of time scales, with no single characteristic scale. Hurst's finding is now recognized as the first example for self-affine fractal behaviour in empirical time series, see e.g. Feder [1988]. In the 1960s, the "Hurst phenomenon" was investigated on a broader empirical basis also for many other natural phenomena [Hurst, Black, and Simaika, 1965, Mandelbrot and Wallis, 1969].

The scaling of the fluctuations with time is reflected by the scaling of the power spectrum $E(f)$ with frequency f , $E(f) \sim f^{-\beta}$. For stationary time series the exponent β is related to the decay of the corresponding autocorrelation function $C(s)$ of the runoffs (see Eq. (1)). For β between 0 and 1, $C(s)$ decays by a power law, $C(s) \sim s^{-\gamma}$, with $\gamma = 1 - \beta$ being restricted to the interval between 0 and 1. In this case, the mean correlation time diverges, and the system is regarded as long-term correlated. For $\beta = 0$, the runoff

data are uncorrelated on large time scales ("white noise"). The exponents β and γ can also be determined from a fluctuation analysis, where the departures from the mean daily runoffs are considered as increments of a random walk process. If the runoffs are uncorrelated, the fluctuation function $F_2(s)$, which is equivalent to the root-mean-square displacement of the random walk, increases as the square root of the time scale s , $F_2(s) \sim \sqrt{s}$. For long-term correlated data, the random walk becomes anomalous, and $F_2(s) \sim s^H$. The fluctuation exponent H is related to the exponents β and γ via $\beta = 1 - \gamma = 2H - 1$. For monofractal data, H is identical with the Hurst exponent.

Recently, many studies using these methods have dealt with scaling properties of hydrological records and the underlying statistics, see e. g. Lovejoy and Schertzer [1991], Turcotte and Greene [1993], Gupta, Mesa, and Dawdy [1994], Tessier et al. [1996], Rodriguez-Iturbe and Rinaldo [1997], Pelletier and Turcotte [1997, 1999], Pandey et al. [1998], Matsoukas, Islam, and Rodriguez-Iturbe [2000], Menabde and Sivapalan [2000], Montanari, Rosso, and Taqqu [2000], Peters et al. [2002], and Livina et al. [2002].

Indeed, all the methods discussed above may fail when trends are present in the system. Trends are systematic deviations from the average runoff that are caused by external processes, e.g. the construction of a water regulation device, the seasonal cycle, or a changing climate (*global warming*). Monotonous trends may lead to an overestimation of the Hurst exponent and thus to an underestimation of γ . It is even possible that uncorrelated data, under the influence of a trend, look like long-term correlated ones when using the above analysis methods. In addition, long-term correlated data cannot simply be detrended by the common technique of moving averages, since this method destroys the correlations on long time scales (above the window size used). Furthermore, it is difficult to distinguish trends from long-term correlations, because stationary long-term correlated time series exhibit persistent behaviour and a tendency to stay close to the momentary value. This causes positive or negative deviations from the average value for long periods of time that might look like a trend.

In the last years, several methods, wavelet techniques (WT) and detrended fluctuation analysis (DFA), have been developed that are able to determine long-term correlations in the presence of trends. For details and applications of the methods to a large number of meteorological, climatological and biological records we refer to Muzy, Bacry, and Arneodo [1991], Peng et al. [1994], Taqqu et al. [1995], Bunde et al. [2000], Kantelhardt et al. [2001], Hu et al. [2001], Arneodo et al.

[2002], *Bunde, Kropp, and Schellnhuber* [2002]. The methods, described in Section 2, consider fluctuations in the cumulated runoffs (often called "profile" or "landscape" of the record). They differ in the way the fluctuations are determined and in the type of polynomial trend that is eliminated in each time window of size s .

In Section 2.5, we apply these detrending methods to study the scaling of the fluctuations $F_2(s)$ of river flows with time s . We focus on 23 runoff records from international river stations spread around the globe and compare the results with those of 18 river stations from southern Germany. We find that all the fluctuations show a pronounced crossover at intermediate scales (usually several months). Below the crossover, for small time windows s , $F_2(s)$ scales as s^H with H close to 1.5, characterizing a highly nonstationary regime similar to Brownian noise. Well above the crossover, at large times, the exponent H varies from river to river between 0.55 and 0.95 in a nonuniversal manner. Our finding is not consistent with the hypothesis that the scaling is universal with an exponent close to 0.75 [Hurst, Black, and Simaika, 1965, see also: Feder, 1988] with the same power law being applicable for all time scales from minutes till centuries [Peters *et al.*, 2002].

The above detrending approaches, however, are not sufficient to fully characterize the complex dynamics of river flows, since they exclusively focus on the variance which can be regarded as the second moment $F_2(s)$ of the full distribution of the fluctuations. Note that the Hurst method actually focuses on the first moment $F_1(s)$. To further characterize a hydrological record, we extend the study to include all moments $F_q(s)$. A detailed description of the method, which is a multifractal generalization of the detrended fluctuation analysis [Kantelhardt *et al.*, 2002] and equivalent to the Wavelet Transform Modulus Maxima (WTMM) method [Arneodo *et al.*, 2002], is given in Section 3. Our approach differs from the multifractal approach introduced into hydrology by Lovejoy and Schertzer (see e.g. Lovejoy and Schertzer [1987,1991], Lavalée *et al.* [1993], Pandey *et al.* [1998]) that was based on the concept of structure functions [Frisch and Parisi, 1985] and on the assumption of the existence of a universal cascade model. Here we perform the multifractal analysis by studying how the different moments of the fluctuations $F_q(s)$ scale with time s , see also Rodriguez-Iturbe and Rinaldo [1997]. We find that at large time scales, $F_q(s)$ scales as $s^{h(q)}$, and a simple functional form with two parameters (a and b), $h(q) = (1/q) - [\ln(a^q + b^q)]/[q \ln(2)]$ describes the scaling exponent $h(q)$ of all moments. On small time scales, however, a stronger multifractality is observed that may be partly related to the seasonal trend. The mean position of the crossover between the two regimes is of the order of several months and increases with q .

II. CORRELATION ANALYSIS

Consider, e. g., a record of daily water runoff values W_i measured at a certain hydrological station. The index i counts the days in the record, $i = 1, 2, \dots, N$. For eliminating the

periodic seasonal trends, we concentrate on the departures $\phi_i = W_i - \bar{W}_i$ from the mean daily runoff \bar{W}_i . \bar{W}_i is calculated for each calendar date i , say 1st of April, by averaging over all years in the runoff series.

The runoff autocorrelation function $C(s)$ describes, how the persistence decays in time. $C(s)$ is defined by

$$C(s) = \langle \phi_i \phi_{i+s} \rangle. \quad (1)$$

The average $\langle \dots \rangle$ is over all pairs with same time lag s . If the ϕ_i are uncorrelated, $C(s)$ is zero for s positive. If correlations exist up to a certain number of days s_\times , the correlation function will be positive up to s_\times and vanish above s_\times . If long-term correlations are present, s_\times diverges, and we observe a power-law decay,

$$C(s) \sim s^{-\gamma}, \quad 0 < \gamma < 1. \quad (2)$$

For large values of s , a direct calculation of $C(s)$ is hindered by the level of noise present in the finite hydrological records, and by nonstationarities in the data. There are several alternative methods for calculating the correlation function in the presence of long-term correlations, which we describe in the following.

A. Power Spectrum Analysis

If the time series is stationary, we can apply standard spectral analysis techniques and calculate the power spectrum $E(f)$ of the time series W_i as a function of the frequency f . For long-term correlated data, we have

$$E(f) \sim f^{-\beta}, \quad (3)$$

where β is related to the correlation exponent γ by

$$\beta = 1 - \gamma. \quad (4)$$

This relation can be derived from the Wiener-Khinchin theorem. If, instead of the W_i the integrated runoff time series $z_n = \sum_{i=1}^n \phi_i$ is Fourier transformed, the resulting power spectrum scales as

$$\tilde{E}(f) \sim f^{-2-\beta}. \quad (5)$$

B. Standard Fluctuation Analysis (FA)

In the standard fluctuation analysis, we consider the "runoff profile"

$$z_n = \sum_{i=1}^n \phi_i, \quad n = 1, 2, \dots, N, \quad (6)$$

and study how the fluctuations of the profile, in a given time window of size s , increase with s . We can consider the profile z_n as the position of a random walker on a linear chain after n

steps. The random walker starts at the origin and performs, in the i th step, a jump of length ϕ_i to the right, if ϕ_i is positive, and to the left, if ϕ_i is negative.

To find how the square-fluctuations of the profile scale with s , we first divide each record of N elements into $N_s = \text{int}(N/s)$ nonoverlapping segments of size s starting from the beginning and N_s nonoverlapping segments of size s starting from the end of the considered runoff series. Then we determine the fluctuations in each segment ν .

In the standard fluctuation analysis, we obtain the fluctuations just from the values of the profile at both endpoints of each segment ν ,

$$F^2(\nu, s) = [z_{\nu s} - z_{(\nu-1)s}]^2, \quad (7)$$

and average $F^2(\nu, s)$ over the $2N_s$ subsequences to obtain the mean fluctuation $F_2(s)$,

$$F_2(s) \equiv \left\{ \frac{1}{2N_s} \sum_{\nu=1}^{2N_s} F^2(\nu, s) \right\}^{1/2}. \quad (8)$$

By definition, $F_2(s)$ can be viewed as root-mean-square displacement of the random walker on the chain, after s steps. For uncorrelated ϕ_i values, we obtain Fick's diffusion law $F_2(s) \sim s^{1/2}$. For the relevant case of long-term correlations, where $C(s)$ follows the power-law behaviour of Eq. (2), $F_2(s)$ increases by a power law [Havlin *et al.*, 1988],

$$F_2(s) \sim s^H, \quad (9)$$

where the fluctuation exponent H is related to the correlation exponent γ and the power-spectrum exponent β by

$$H = 1 - \gamma/2 = (1 + \beta)/2. \quad (10)$$

For power-law correlations decaying faster than $1/s$, we have $H = 1/2$ for large s values, like for uncorrelated data.

We like to note that the standard fluctuation analysis is somewhat similar to the rescaled range analysis introduced by Hurst (for a review see, e. g., Feder [1988]), except that it focusses on the second moment $F_2(s)$ while Hurst considered the first moment $F_1(s)$. For monofractal data, H is identical to the Hurst exponent \tilde{H} . The common disadvantage of both methods is, that they are strongly affected by non-stationarities in the record, such as simple polynomial trends, which may lead to spurious results for the correlation exponent. In addition, both methods cannot be used to detect fluctuation exponents greater than one that occur, for example, when the data in the signal resemble the profile of a random walk. In this case, both FA and R/S analysis yield (as an artefact of their construction) $F(s) \sim s$ for any record with H respectively \tilde{H} above one. We come back to this point when describing Fig. 2.

Next we describe methods that are able to determine long-term correlations in the presence of trends and other non-stationarities.

C. The Detrended Fluctuation Analysis (DFA)

There are different orders of DFA that are distinguished by the way the trends in the data are eliminated. In lowest order (DFA1) we determine, for each segment ν , the best *linear* fit of the profile, and identify the fluctuations by the variance $F^2(\nu, s)$ of the profile from this straight line. This way, we eliminate the influence of possible linear trends on scales larger than the segment. Note that linear trends in the profile correspond to patch-like trends in the original record. DFA1 has been proposed originally by Peng *et al.* [1994] when analyzing correlations in DNA. It can be generalized straightforwardly to eliminate higher order trends [Bunde *et al.*, 2000, Kantelhardt *et al.*, 2001, Hu *et al.*, 2001].

In second order DFA (DFA2) one calculates the variances $F^2(\nu, s)$ of the profile from best *quadratic* fits of the profile, this way eliminating the influence of possible linear and parabolic trends on scales larger than the segment considered. In general, in the n thorder DFA technique, we calculate the variances of the profile from the best n th-order polynomial fit, this way eliminating the influence of possible $(n-1)$ th-order trends on scales larger than the segment size.

Explicitly, we calculate the best polynomial fit $y_\nu(i)$ of the profile in each of the $2N_s$ segments ν and determine the variance

$$F^2(\nu, s) \equiv \frac{1}{s} \sum_{i=1}^s [z_{(\nu-1)s+i} - y_\nu(i)]^2. \quad (11)$$

Then we employ Eq. (8) to determine the mean fluctuation $F_2(s)$.

Since FA and the various stages of the DFA have different detrending capabilities, a comparison of the fluctuation functions obtained by FA and DFA_n can yield insight into both long-term correlations and types of trends. This cannot be achieved by the conventional methods, like the spectral analysis.

D. Wavelet Transform (WT)

The wavelet methods we employ here are based on the determination of the mean values $\bar{z}_\nu(s)$ of the profile in each segment ν (of length s), and the calculation of the fluctuations between neighbouring segments. The different order techniques we have used in analyzing runoff fluctuations differ in the way the fluctuations between the average profiles are treated and possible nonstationarities are eliminated.

(i) In the first-order wavelet method (WT0), one simply determines the fluctuations from the first derivative

$$F^2(\nu, s) = [\bar{z}_\nu(s) - \bar{z}_{\nu+1}(s)]^2. \quad (12)$$

WT0 corresponds to FA where constant trends in the profile of a hydrological station are eliminated, while linear trends are not eliminated.

(ii) In the second-order wavelet method (WT1), one determines the fluctuations from the second derivative

$$F^2(\nu, s) = [\bar{z}_\nu(s) - 2\bar{z}_{\nu+1}(s) + \bar{z}_{\nu+2}(s)]^2. \quad (13)$$

So, if the profile consists of a trend term linear in s and a fluctuating term, the trend term is eliminated. Regarding trend elimination, WT1 corresponds to DFA1.

(iii) In the third-order wavelet method (WT2), one determines the fluctuations from the third derivative

$$F^2(\nu, s) = [\bar{z}_\nu(s) - 3\bar{z}_{\nu+1}(s) + 3\bar{z}_{\nu+2}(s) - \bar{z}_{\nu+3}(s)]^2. \quad (14)$$

By definition, WT2 eliminates linear and parabolic trend terms in the profile. In general, in WT_n we determine the fluctuations from the $(n+1)$ th derivative, this way eliminating trends described by n th-order polynomials in the data.

Methods (i-iii) are called wavelet methods, since they can be interpreted as transforming the profile by discrete wavelets representing first-, second- and third-order cumulative derivatives of the profile. The first-order wavelets are known in the literature as Haar wavelets. One can also use different shapes of the wavelets (e.g. Gaussian wavelets with width s), which have been used by Arneodo *et al.* [2002] to study, for example, long-range correlations in DNA.

We note that the first-order wavelet method has the same deficiency as the FA and R/S method: Apart from the fact that trends are not eliminated, records described by H greater than one cannot be analysed properly, since for all $H > 1$ the WT_0 yields spuriously $H = 1$. Since the various stages of the wavelet methods WT_0 , WT_1 , WT_2 , etc. have different detrending capabilities, a comparison of their fluctuation functions can yield insight into both long-term correlations and types of trends.

At the end of this section, before describing the results of the FA, DFA, and WT analysis, we note that for very large s values, $s > N/4$ for FA and DFA and $s > N/10$ for WT, the fluctuation function becomes inaccurate due to statistical errors. Hence, we concentrate on s values lower than $s_{\max} = N/4$ for FA and DFA and $s_{\max} = N/10$ for WT.

E. Results

In our study we analyzed 41 runoff records, 18 of them are from the southern part of Germany, and the rest is from North- and South America, Africa, Australia, Asia and Europe (see Tables 1 and 2). We begin the analysis with the runoff record for the river Weser in the northern part of Germany, which is the longest record (171 years) in this study. Qualitatively, persistence can be seen already in plots of the departures $\phi_i = W_i - \bar{W}_i$ from the mean daily runoffs \bar{W}_i , as shown in Fig. 1(a) for two successive years from the middle of the record. The persistence is represented by relatively large patches of positive and negative values of ϕ_i . Indeed, when the data are randomly shuffled and again two successive years from the middle of the shuffled record are plotted, the large patches disappear, as seen in Fig. 1(d).

River name	Station name	Index	Period of observation (y)	Basin area (km ²)
Barron River	Myola, Australia	I1	79	1940
Columbia River	The Dallas, USA	I2	114	613 830
Danube	Orsova, Romania	I3	151	576 232
Dvina	UST-Pinega, Russia	I4	89	348 000
Fraser River	Hope, USA	I5	84	217 000
Gaula	Haga Bru, Norway	I6	90	3080
Johnston River	Upstream Central Mill, Australia	I7	74	390
Labe	Decin, Czechia	I8	102	51 104
Maas	Borgharen, Netherland	I9	80	21 300
Mary River	Miva, Australia	I10	76	4830
Mitta Mitta River	Hinnomunjie, Australia	I11	67	1530
Niger	Koulakoro, Mali	I12	79	120 000
Orinoco	Puente Angostura, Venezuela	I13	65	836 000
Rhein	Rees, Germany	I14	143	159 680
Severn	Bewdley, England	I15	71	4330
Susquehanna	Harrisburg, USA	I16	96	62 419
Tana	Polmak, Norway	I17	51	14 005
Themse	Kingston, England	I18	113	9948
Weser	Vlotho, Germany	I19	171	17 618
Zaire	Kinshasa, Zaire	I20	81	3 475 000
Grand River	Gallatin, USA	I21	72	5830
Susquehanna	Marietta, USA	I22	61	67 310
Mississippi	St. Louis, USA	I23	59	1 805 000

TABLE I. Table of investigated international river basins (data from Global Runoff Data Center (GRDC), Koblenz, Germany). In addition to the river and station name, we report the duration of the investigated daily record and the size of the basin area, as well as the index codes we assigned to the rivers.

River name	Station name	Index	Period of observation (y)	Basin area (km ²)
Amper	Fürstenfeldbruck	B1	77	1235
Donau (Danube)	Achleiten	B2	97	76 653
Donau (Danube)	Beuron	B3	70	1309
Donau (Danube)	Donauwörth	B4	74	15 037
Donau (Danube)	Kehlheim	B5	97	22 950
Isar	Bad Tölz	B6	39	1554
Jagst	Untergriesheim	B7	73	1826
Kinzig	Schwaibach	B8	82	921
Loisach	Kochel	B9	87	684
Kocher	Stein	B10	111	1929
Murg	Rotenfels	B11	77	469
Neckar	Horb	B12	65	1118
Neckar	Plochingen	B13	79	3995
Tauber	Bad Mergentheim	B14	66	1018
Wertach	Biessenhofen	B15	77	450
Würm	Leutstetten	B16	77	413
Wutach	Oberlauchringen	B17	85	1129
Vils	Grafenmühle	B18	58	1436

TABLE II. Table of investigated river basins in southern Germany.

Figures 1(b) and (e) show the corresponding profiles, as defined in Eq. (6), for the whole duration of the record. The persistence of the data leads to strong fluctuations in Fig. 1(b). In contrast, the profile becomes much smoother when the persistence is removed by randomly shuffling the data [Fig. 1(d)]. Figure 1(c) shows the fluctuation functions $F_2(s)$ obtained from FA and DFA1-DFA5. In the log-log plot, the curves are approximately straight lines for s above 30 days, with a slope $H \approx 0.75$. This result for the Weser suggests, that there exists long-term persistence expressed by the power-law decay of the correlation function, with an exponent $\gamma \approx 0.5$ [see Eq. (9)].

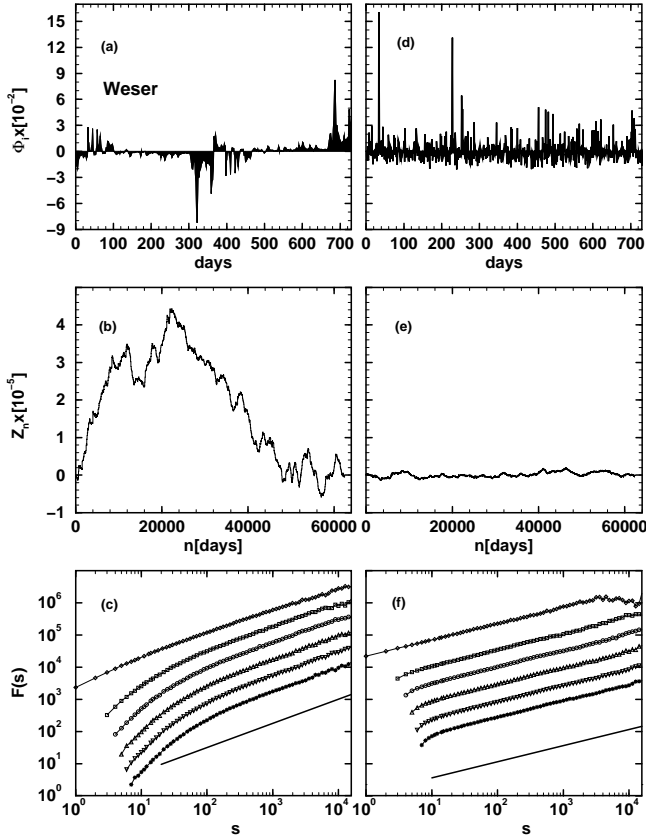


FIG. 1. (a) Daily runoff departures $\phi_i = W_i - \bar{W}_i$ from the mean daily runoff \bar{W}_i for the river Weser, measured from 1 January 1823 till 31 December 1824 by the hydrological station Vlotho in Germany. (b) The runoff profile $z_n = \sum_{i=1}^n \phi_i$ for the Weser, for the entire 171 yr (1823-1993). (c) The fluctuation function $F(s) = F_2(s)$ obtained (i) from the standard fluctuation analysis (FA, diamonds), (ii) from the first order detrended fluctuation analysis (DFA1, squares), (iii) from the second, third, forth, and fifth order DFA (DFA2-DFA5, circles, triangles up, triangles down, and filled circles, respectively). In the log-log plot, the curves appear to be approximate straight lines for time scales s above 100 days, and their slope $H \approx 0.75$ (shown as straight line in the figure) is related to the correlation exponent γ by $\gamma = 2 - 2H$, yielding $\gamma = 0.5$. (d)-(f) The analog curves to (a)-(c), respectively, when the ϕ_i are randomly shuffled. In this case, due to the shuffling, the correlations have been removed, and the fluctuation function $F_2(s)$ is proportional to $s^{1/2}$, as indicated by the straight line with slope 1/2 in (f).

To show that the slope $H \approx 0.75$ is due to long-term correlations and not due to a broad probability distribution (Joseph- versus Noah-Phenomenon, see *Mandelbrot and Wallis* [1968]), we have eliminated the correlations by randomly shuffling the ϕ_i . This shuffling has no effect on the probability distribution function of the ϕ_i . Figures 1(d)-(f) show the effect of shuffling on (d) the daily runoff fluctuations ϕ_i , (e) the profile, and (f) the fluctuation functions. By comparing Figs. 1(a)-(c) with 1(d)-(f), we see the effect of correlations: The uncorrelated ϕ_i are less patchy, the uncorrelated profile shows much smaller fluctuations, and the exponent H characterizing the fluctuations in the shuffled uncorrelated sequence is 1/2, as expected.

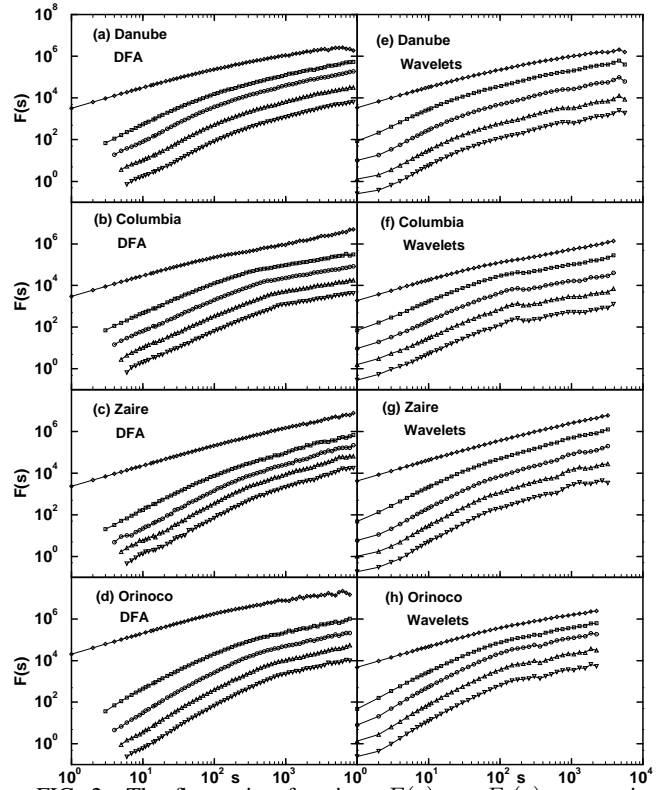


FIG. 2. The fluctuation functions $F(s) = F_2(s)$ versus time scale s obtained from FA and DFA1-DFA4 in double logarithmic plots for four additional representative hydrological stations: (a) the Danube in Orsova, Romania, (b) the Columbia River in The Dallas, USA, (c) the Zaire in Kinshasa, Zaire, and (d) the Orinoco in Puente Angostura, Venezuela. For the different analysis methods, we used the same symbols as in Figs. 1(c), 1(f). For $s > 100 - 500$ days, the curves obtained by the DFA methods appear to be approximate straight lines, with slopes H depending on the specific river, $H \simeq 0.85$ for Danube, $H \simeq 0.59$ for Columbia, $H \simeq 0.95$ for Zaire and $H \simeq 0.73$ for Orinoco. (e-h) The fluctuation functions $F_2(s)$ obtained for the same rivers as in (a-d), (i) from the first order wavelet fluctuation analysis (WT0, diamonds), (ii) from the second, third, forth, and fifth order wavelet analysis (WT1-WT4, squares, circles, triangles up, and triangles down, respectively). The position of the crossover to straight line scaling behaviour can be determined best using the DFA1 and WT1-4 curves, since it is systematically moved to larger scales for DFA2-DFA4. Thus, the crossover occurs at $s_x \approx 30 - 100$ days.

Figure 2 shows the fluctuation functions of 4 more rivers, from Europe, North America, Africa and South America. The panels on the left side show the FA and DFA1-4 curves, while the panels on the right show the results from the analogous wavelet analysis WT0-WT4. All curves show a remarkable crossover between 30 and 100 days, which can be estimated best from the DFA1 and WT1-4 curves. A similar crossover has been reported by *Tessier et al.* [1996] for small French rivers without artificial dams or reservoirs. Below and above the crossover time s_{\times} , the fluctuation functions (from DFA1-4 and WT1-4) show power-law behaviour, with exponents slightly above 1.5 below s_{\times} and exponents $H \simeq 0.85$ for Danube, $H \simeq 0.59$ for Columbia, $H \simeq 0.95$ for Zaire and $H \simeq 0.73$ for Orinoco above s_{\times} .

Accordingly, there is no universal scaling behaviour since the long-term exponents vary strongly from river to river. This finding is consistent with the observation that small and large basins exhibit a quite different scaling behaviour [*Gupta, Mesa, and Dawdy, 1994*]. In addition, there exist different mechanisms for floods where each may induce different scaling. For example, rain induced floods and snow induced floods may introduce different scaling [*Gupta and Dawdy, 1995*].

This nonuniversal feature found in rivers should be compared with climate records, where universal long-term persistence of temperature records at land stations were observed [*Koscielny-Bunde et al., 1996, 1998, Pelletier and Turcotte, 1997, Pelletier, 1997, Pelletier and Turcotte, 1999, Talkner and Weber, 2000*]. Recently these results have been applied to evaluate the performance of global climate models [*Govindan et al., 2002*]. In contrast to the temperature records, the hydrological records are usually characterized by two different scaling regimes separated by a crossover time s_{\times} that in Fig. 2 varies between 30 and 100 days. Below s_{\times} , in the short time regime, the data are non-stationary, being characterized by a scaling exponent above 1.5. Above s_{\times} , the data are long-term power-law correlated with exponents between 0.55 and 0.95 (see also the histogram in Fig. 4).

Figure 2 shows clearly the deficiencies of the FA and WT0 method discussed above that is also shared by Hursts R/S -method. Below the crossover times, the FA and WT0 curves are straight lines in the log-log plot with slope 1, yielding the spurious result $H = 1$ for fluctuations that are actually described by $H \simeq 1.5$ at small times s . We like to note that for detecting nonstationary behaviour ($H > 1$) within FA, WT0 and R/S analysis, one has to study the increment series $\Delta\phi_i = \phi_{i+1} - \phi_i$ of the original series ϕ_i . In this case, ϕ_i is the profile of the increment series $\Delta\phi_i$. When analyzing the increment series, H will be decreased by one: If the ϕ_i have a fluctuation exponent H close to 1.5, the fluctuation exponent of the $\Delta\phi_i$ is close to 0.5. Indeed, when analyzing the $\Delta\phi_i$ record using FA and WT0, we obtained an exponent close to 0.5 below the crossover.

When looking at the position of the crossover, one notices also a (minor) deficiency of the DFA methods: With increasing order of DFA, the crossover shifts towards larger values of s [*Kantelhardt et al., 2001, Hu et al., 2001*]. For best estimate of the real crossover, it is better to choose the various wavelet

methods WT1-4, where the position of the crossover is almost unchanged.

Figure 3 shows the fluctuation functions for two rivers that are different from the others, (a) for a river that is rather dry in the summer (Mary River, Australia) and (b) a river (Gaula River, Norway) that is frozen in the winter. For the Mary river, the crossover time s_{\times} is only about 5 days and the long-term exponent $H \simeq 0.60$ is well below the average value. For the Gaula river, the crossover time is about 30 days. The long-term correlations are not pronounced ($H = 0.55$) and even hard to distinguish from the uncorrelated case $H = 0.5$. We obtained similar results for the other two "frozen" rivers (Tana from Norway and Dvina from Russia) that we analysed. For interpreting this distinguished behaviour of the frozen rivers we like to note that on permafrost ground the lateral inflow (and hence the indirect contribution of the water storage in the catchment basin) contributes to the runoffs in a different way than on normal ground. Our results suggest that the contribution of snow melting leads to less correlated runoffs than the contribution of rainfall.

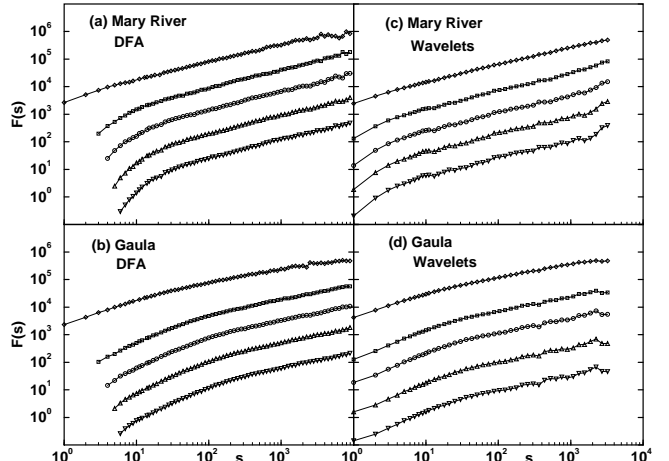


FIG. 3. The fluctuation functions $F(s) = F_2(s)$ versus s obtained from (a,b) FA and DFA1-DFA4 and (c,d) WT0-WT4 for two rivers that are either rather dry in the summer (Mary River, Australia (a,c)) or frozen in the winter (Gaula River, Norway, (b,d)). The long-term correlations are not pronounced ($H = 0.60$ and $H = 0.55$, respectively) and the crossover times s_{\times} are rather small (5 days and 30 days, respectively).

Figure 4 and Table 3 summarize our results for the long-term exponents H we obtained for the international rivers (I1-I23) and the rivers from South Germany (B1-B18). As can be seen in the figure, the exponents spread from 0.55 to 0.95 covering the whole range from very weak to very strong correlations. Since the correlation exponent γ is related to H by $\gamma = 2 - 2H$, the exponent γ spreads from almost 0 to almost 1, covering the whole range of long-term correlations. Note that the rivers within a localized area (as South Germany) tend to have nearly the same range of exponents as the international rivers. The three "frozen" rivers in our study have the lowest values of H .

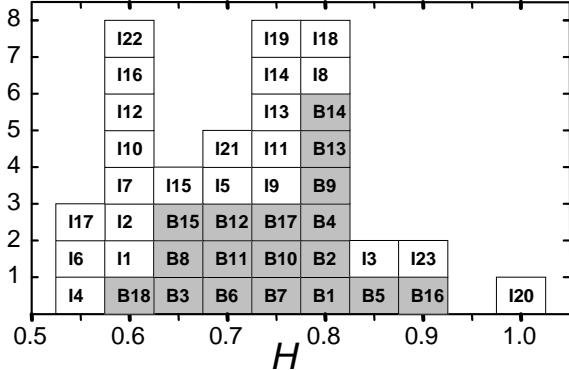


FIG. 4. Histogram of the long-term fluctuation exponents H for all international records (I1-I23) and all records from south Germany (B1-B18, grey) that we analyzed. Each box represents the result for one hydrological station. The three "frozen" rivers in our study have the lowest values of H .

III. MULTIFRACTAL ANALYSIS

A. Method

For a further characterization of hydrological records it is meaningful to extend Eq. (8) by considering the more general fluctuation functions [Barabasi and Vicsek, 1991],

$$F_q(s) = \left\{ \frac{1}{2N_s} \sum_{\nu=1}^{2N_s} |z_{\nu s} - z_{(\nu-1)s}|^q \right\}^{1/q}. \quad (15)$$

where the variable q can take any real value except zero. For $q = 2$, the standard fluctuation analysis, Eqs. (7) and (8), is retrieved. The question is, how the fluctuation functions depend on q and how this dependence is related to multifractal features of the record.

In general, the multifractal approach is introduced by the partition function

$$Z_q(s) \equiv \sum_{\nu=1}^{N_s} |z_{\nu s} - z_{(\nu-1)s}|^q \sim s^{\tau(q)}, \quad (16)$$

where $\tau(q)$ is the Renyi scaling exponent. A record is called 'monofractal', when $\tau(q)$ depends linearly on q ; otherwise it is called multifractal.

It is easy to verify that $Z_q(s)$ is related to $F_q(s)$ by

$$F_q(s) = \left\{ \frac{1}{N_s} Z_q(s) \right\}^{1/q}. \quad (17)$$

Accordingly, Eq. (16) implies

$$F_q(s) \sim s^{h(q)}, \quad (18)$$

where

$$h(q) = [\tau(q) + 1]/q. \quad (19)$$

Thus, $h(q)$ defined in Eq. (18) is directly related to the classical multifractal scaling exponents $\tau(q)$.

In general, the exponent $h(q)$ may depend on q . Since for stationary records, $h(1)$ is identical to the well-known Hurst exponent \tilde{H} (see e. g. Feder [1988]), we will call the function $h(q)$ generalized Hurst exponent. For monofractal self-affine time series, $h(q)$ is independent of q , since the scaling behaviour of the variances $F^2(\nu, s)$ is identical for all segments ν , and the averaging procedure in Eq. (15) will give just this identical scaling behaviour for all values of q . Only if small and large fluctuations scale differently, there will be a significant dependence of $h(q)$ on q : If we consider positive values of q , the segments ν with large variance $F^2(\nu, s)$ (i. e. large deviations from the corresponding fit) will dominate the average $F_q(s)$. Thus, for positive values of q , $h(q)$ describes the scaling behaviour of the segments with large fluctuations. Usually the large fluctuations are characterized by a smaller scaling exponent $h(q)$ for multifractal series. On the contrary, for negative values of q , the segments ν with small variance $F^2(\nu, s)$ will dominate the average $F_q(s)$. Hence, for negative values of q , $h(q)$ describes the scaling behaviour of the segments with small fluctuations, which are usually characterized by a larger scaling exponent.

In the hydrological literature (see, e. g., Rodriguez-Iturbe and Rinaldo [1997] and Lavee et al. [1993]) one often considers the generalized mass variogram $C_q(\lambda)$,

$$C_q(\lambda) \equiv \langle |z_{i+\lambda} - z_i|^q \rangle \sim \lambda^{K(q)}. \quad (20)$$

Comparing Eqs. (15), (18), and (20) one can verify easily that $K(q)$ and $h(q)$ are related by

$$h(q) = K(q)/q. \quad (21)$$

Another way to characterize a multifractal series is the singularity spectrum $f(\alpha)$, that is related to $\tau(q)$ via a Legendre transform (see, e.g., Feder [1988], Peitgen, Jürgens, and Saupe [1992], Rodriguez-Iturbe and Rinaldo [1997]),

$$\alpha = \frac{d\tau(q)}{dq} \quad \text{and} \quad f(\alpha) = q\alpha - \tau(q). \quad (22)$$

Here, α is the singularity strength or Hölder exponent, while $f(\alpha)$ denotes the dimension of the subset of the series that is characterized by α . Using Eq. (19), we can directly relate α and $f(\alpha)$ to $h(q)$,

$$\alpha = h(q) + q \frac{dh(q)}{dq} \quad \text{and} \quad f(\alpha) = q[\alpha - h(q)] + 1. \quad (23)$$

The strength of the multifractality of a time series can be characterized by the difference between the maximum and minimum values of α , $\alpha_{\max} - \alpha_{\min}$. When $q \frac{dh(q)}{dq}$ approaches zero for q approaching $\pm\infty$, then $\Delta\alpha = \alpha_{\max} - \alpha_{\min}$ is simply given by $\Delta\alpha = h(-\infty) - h(\infty)$.

The multifractal analysis described above is a straightforward generalization of the fluctuation analysis and therefore has the same problems: (i) Monotonous trends in the record may lead to spurious results for the fluctuation exponent $h(q)$

which in turn leads to spurious results for the correlation exponent γ . (ii) Nonstationary behaviour characterized by exponents $h(q) > 1$ cannot be detected by the simple method since the method cannot distinguish between exponents > 1 and always will yield $F_2(s) \sim s$ in this case (see above). To overcome these drawbacks the multifractal detrended fluctuation analysis (MF-DFA) has been introduced recently [Kantelhardt *et al.*, 2002, see also Koscielny-Bunde *et al.*, 1998, Weber and Talkner, 2001]. According to [Kantelhardt *et al.*, 2002], the method is as accurate as the wavelet methods. Thus, we have used MF-DFA for the multifractal analysis here. In the MF-DFA, one starts with the DFA-fluctuations $F_\nu^2(s)$ as obtained in Eq. (11). Then, we define in close analogy to Eqs. (8) and (15) the generalized fluctuation function,

$$F_q(s) \equiv \left\{ \frac{1}{2N_s} \sum_{\nu=1}^{2N_s} [F^2(\nu, s)]^{q/2} \right\}^{1/q}. \quad (24)$$

Again, we can distinguish MF-DFA1, MF-DFA2, etc. according to the order of the polynomial fits involved.

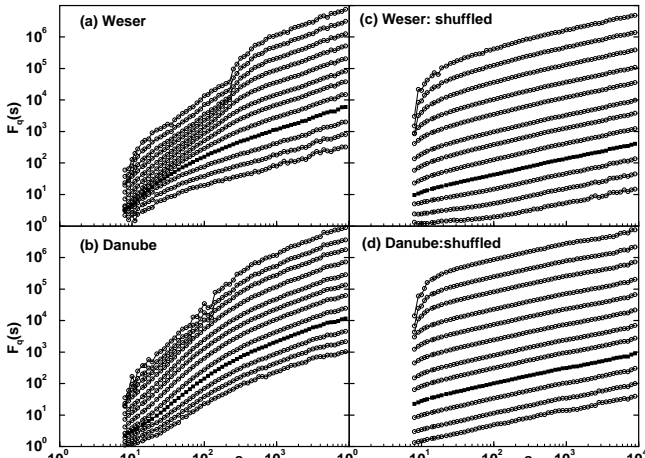


FIG. 5. The multifractal fluctuation functions $F_q(s)$ versus time scale s obtained from multifractal DFA4 for two representative hydrological stations: (a) river Weser in Vlotho, Germany and (b) river Danube in Orsova, Romania. The curves correspond to different values of q , $q = -10, -6, -4, -2, -1, -0.2, 0.2, 0.4, 1, 2, 4, 6, 10$ (from the top to the bottom) and are shifted vertically for clarity. The curves for $q = 2$, which are marked by the full symbols, are identical to the curves for DFA4 in Figs. 1(c) and 2(a), respectively. Above the crossover the $F_q(s)$ functions are straight lines in the double logarithmic plot, and the slopes increase slightly when going from high positive moments towards high negative moments. This is the signature of weak multifractality. (c,d) The analog curves to (a,b), respectively, when the ϕ_i are randomly shuffled. Due to the shuffling, all correlations have been removed, and all multifractal fluctuation functions $F_q(s)$ are proportional to $s^{1/2}$.

B. Multifractal Scaling Plots

We have performed a multifractal analysis of all 41 rivers. We obtained that MF-DFA2-5 yield similar results for the

fluctuation function $F_q(s)$. We have also cross checked the results by using the Wavelet Transform Modulus Maxima (WTMM) method [Muzy, Bacry, and Arneodo, 1991, Arneodo, 2002], and always find agreement within the error bars. Therefore, we present here only the results of MF-DFA4. Figure 5(a,b) shows two representative examples for the fluctuation functions $F_q(s)$, for (a) the Weser river and (b) the Danube river. The standard fluctuation function $F_2(s)$ is plotted in full symbols. The crossover in $F_2(s)$ that was discussed in Sect. II E can be also seen in the other moments $F_q(s)$. The position of the crossover increases monotonously with decreasing q and the crossover becomes more pronounced. The DFA4 curves shown here slightly overestimate the position of the crossover, as mentioned before. We are interested in the asymptotic behaviour of $F_q(s)$ at large times s . One can see clearly that above the crossover, the $F_q(s)$ functions are straight lines in the double logarithmic plot, and the slopes increase slightly when going from high positive moments towards high negative moments (from the bottom to the top). For the Weser, for example, the slope changes from 0.65 for $q = 10$ to 0.9 for $q = -10$ (see also Fig. 7(b)). The monotonous increase of the slopes, $h(q)$, is the signature of multifractality.

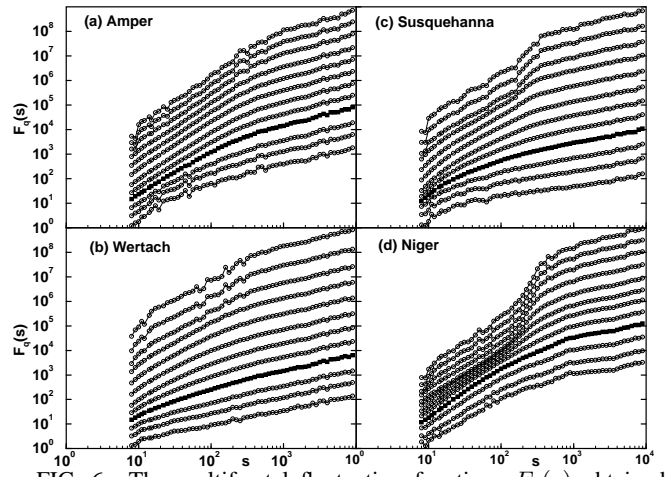


FIG. 6. The multifractal fluctuation functions $F_q(s)$ obtained from multifractal DFA4 for four additional hydrological stations: (a) Amper in Fürstenfeldbruck, Germany, (b) Wertach in Biessenhofen, Germany, (c) Susquehanna in Harrisburg, USA, (d) Niger in Koulikoro, Mali. The q -values are identical to those used in Fig. 5.

When the data are shuffled (see Figs. 5(c,d)), all functions $F_q(s)$ increase asymptotically as $F_q(s) \sim s^{1/2}$. This indicates that the multifractality vanishes under shuffling. Accordingly the observed multifractality originates in the long-term correlations of the record and is not caused by singularities in the distribution of the daily runoffs (see also Mandelbrot and Wallis [1968]). A reshuffling-resistant multifractality would indicate a 'statistical' type of non-linearity [Sivapalan, Jothityangkoon, and Menabde, 2002]). We obtain similar patterns for all rivers. Figure 6 shows four more examples; Figs. 6(a,b) are for two rivers (Amper and Wertach) from southern Germany, while Figs. 6(c,d) are for Niger and Susquehanna

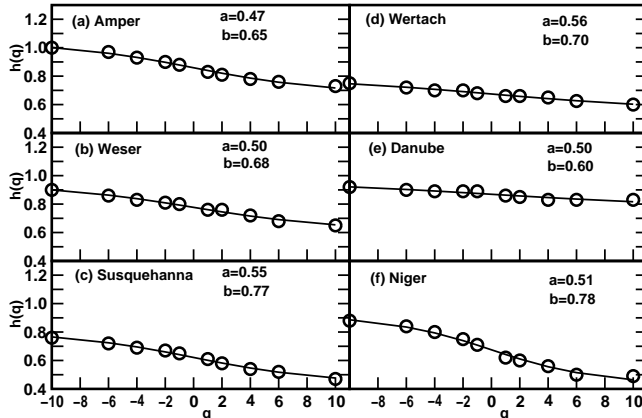


FIG. 7. The generalized Hurst exponents $h(q)$ for the six representative daily runoff records analyzed in Figs. 5 and 6: (a) Amper in Fürstenfeldbruck, Germany, (b) Weser in Vlotho, Germany, (c) Susquehanna in Harrisburg, USA, (d) Wertach in Biessenhofen, Germany, (e) Danube in Orsova, Romania, and (f) Niger in Koulikoro, Mali. The $h(q)$ values have been determined by straight line fits of $F_q(s)$ on large time scales. The error bars of the fits correspond to the size of the symbols. The lines are obtained by fits of the two-parameter binomial model that is described in Sect. III C. The resulting model parameters a and b are reported in the Figures. All fits are consistent with the data within the error bars.

From the asymptotic slopes of the curves in Figs. 5(a,b) and 6(a-d), we obtain the generalized Hurst-exponents $h(q)$, which are plotted in Fig. 7 (circles). The line is obtained by a modification of the two-parameter binomial model that is described in Sect. III C. The model yields

$$h(q) = \frac{1}{q} - \frac{\ln[a^q + b^q]}{q \ln 2}, \quad (25)$$

or

$$K(q) = 1 + \tau(q) = 1 - \frac{\ln[a^q + b^q]}{\ln 2}. \quad (26)$$

We have fitted the $h(q)$ spectra in the range $-10 \leq q \leq 10$ for all 41 runoff series with Eq. (25), see Fig. 7. The results for the two parameters a and b (together with $H = h(2)$ and $\Delta\alpha$ (see below)) are shown in Table 3. In each single case, the q dependence of $h(q)$ for positive and negative values of q can be characterized well by the two parameters, and all fits remain within the error bars of the $h(q)$ values.

From $h(q)$ we obtain $\tau(q)$ (Eq. (19)) and the singularity spectrum $f(\alpha)$ (Eq. (23)). Figure 8 shows two typical examples for the Danube and the Niger. The width of $f(\alpha)$ taken at $f = 0$ characterizes the strength of the multifractality. Since both widths are very different, the strength of the multifractality of river runoffs is not universal.

In order to characterize and to compare the strength of the multifractality for several time series we use as parameter the width of the singularity spectrum $f(\alpha)$ [see Eqs. (22) and (23)] at $f = 0$, which corresponds to the difference of the maximum and the minimum value of α . In the binomial multifractal model, this parameter is given by

$$\Delta\alpha = \frac{\ln a - \ln b}{\ln 2}. \quad (27)$$

The distribution of the $\Delta\alpha$ values we obtained from Eq. (27) is shown in the histogram in Fig. 9. The histogram shows that there are rivers with quite strong multifractal fluctuations, i.e. large $\Delta\alpha$, and one with almost vanishing multifractality, i.e. $\Delta\alpha \approx 0$. The distribution of the multifractality strengths within the local area of southern Germany (grey boxes in Fig. 9) is also quite broad, but definitely not as broad as for the international runoff records from all rivers around the globe.

Index	$h(2)$	a	b	$\Delta\alpha$
I1	0.60	0.50	0.79	0.65
I2	0.59	0.54	0.76	0.50
I3	0.85	0.50	0.60	0.26
I4	0.56	0.53	0.79	0.58
I5	0.69	0.53	0.70	0.38
I6	0.55	0.57	0.77	0.43
I7	0.58	0.52	0.78	0.58
I8	0.80	0.45	0.68	0.61
I9	0.76	0.49	0.68	0.48
I10	0.60	0.52	0.78	0.57
I11	0.75	0.47	0.68	0.53
I12	0.60	0.51	0.78	0.62
I13	0.73	0.50	0.69	0.46
I14	0.76	0.52	0.65	0.32
I15	0.63	0.54	0.73	0.43
I16	0.58	0.55	0.77	0.48
I17	0.56	0.50	0.81	0.69
I18	0.80	0.47	0.67	0.51
I19	0.76	0.50	0.68	0.43
I20	1.00	0.50	0.50	0.00
I21	0.72	0.42	0.76	0.87
I22	0.60	0.53	0.79	0.57
I23	0.91	0.44	0.61	0.48
B1	0.81	0.47	0.65	0.47
B2	0.82	0.49	0.63	0.35
B3	0.65	0.53	0.72	0.45
B4	0.81	0.49	0.63	0.37
B5	0.85	0.48	0.63	0.39
B6	0.68	0.53	0.71	0.41
B7	0.76	0.45	0.69	0.61
B8	0.67	0.52	0.72	0.47
B9	0.82	0.48	0.65	0.44
B10	0.75	0.53	0.64	0.26
B11	0.70	0.53	0.70	0.41
B12	0.68	0.44	0.75	0.78
B13	0.80	0.49	0.65	0.39
B14	0.80	0.44	0.70	0.68
B15	0.66	0.56	0.70	0.31
B16	0.90	0.39	0.66	0.77
B17	0.75	0.52	0.67	0.37
B18	0.61	0.50	0.78	0.62

TABLE III. Table of the fitting results for all international records (I1-I23) and all records from south Germany (B1-B18) that we analyzed. The values of $H = h(2)$ have been obtained by fits to $F_2(s)$ calculated with DFA4 for long time scales s above the crossover. The parameters a and b have been determined by fits of Eq. (25) to the values of the generalized Hurst exponents $h(q)$ as illustrated in Fig. 7. The $\Delta\alpha$ values that characterize the strength of the multifractality follow from Eq. (27).

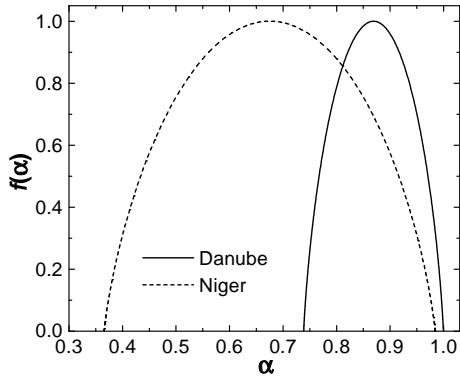


FIG. 8. The multifractal spectra $f(\alpha)$ for two representative runoff records (a) the Danube in Orsova, Romania and (b) Niger in Koulikoro, Mali. Here, α is the singularity strength or Hölder exponent, while $f(\alpha)$ denotes the dimension of the subset of the series that is characterized by α . The spectra have been determined by applying the Legendre transform, Eq. (23), to the model curves fitted to the $h(q)$ results in Figs. 7(e) and (f).

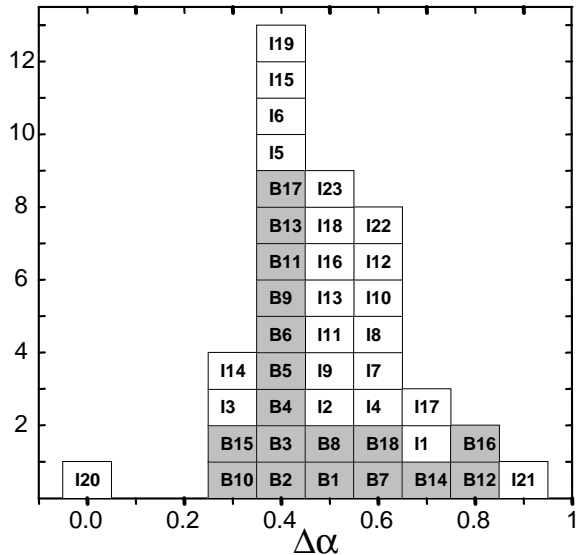


FIG. 9. Histogram of the widths $\Delta\alpha$ of the $f(\alpha)$ spectra for all international records (I1-I23) and all records from south Germany (B1-B18, grey) that we analyzed. The parameter $\Delta\alpha$ is defined in Eq. (27) and characterizes the multifractality strengths, $\Delta\alpha \approx 0$ indicating monofractal behaviour. Each box represents the result for one hydrological station.

Our results for $K(q) = 1 + \tau(q)$ (see Eq. (26) and Table 3) may be compared with the ansatz

$$K(q) = (H' + 1)q - \frac{C_1}{\alpha' - 1}(q^{\alpha'} - q) \quad q \geq 0 \quad (28)$$

with the three parameters H' , C_1 , and α' , that has been used by Lovejoy, Schertzer, and coworkers [Schertzer and Lovejoy, 1987; Lovejoy and Schertzer, 1991, Lavallee *et al.*, 1993, Tessier *et al.*, 1996, Pandey *et al.*, 1998] successfully to describe the multifractal behaviour of rainfall and runoff records. The definition of $K(q)$ we used in this paper is taken from Rodriguez-Iturbe and Rinaldo [1997] and differs slightly from

their definition. We like to note that Eq. (26) for $K(q)$ is not only valid for positive q values, but also for negative q values. This feature allows us to determine numerically the full singularity spectrum $f(\alpha)$. In the analysis we focused on long time scales, excluding the crossover regime, and used detrending methods. We consider it as particularly interesting that only two parameters a and b or, equivalently, H and $\Delta\alpha$, are sufficient to describe $\tau(q)$ and $K(q)$ for positive as well as negative q values. This strongly supports the idea of 'universal' multifractal behaviour of river runoffs as suggested by Lovejoy and Schertzer.

C. Extended Binomial Cascade Model

In order to characterize the multifractal spectra with a minimum number of parameters, we consider the binomial multifractal model, see e.g. Feder [1988], Barabasi and Vicsek [1991], Peitgen *et al.* [1992], and Kantelhardt *et al.* [2002]. The model is based on a multiplicative cascade process. In this process, a record ϕ_k of length $N = 2^{n_{\max}}$ is constructed recursively:

In generation $n = 0$, the record elements are constant, $\phi_k = 1$ for all $k = 1, \dots, N$. In the first step of the cascade (generation $n = 1$) the first half of the series is multiplied by a factor a and the second half of the series is multiplied by a factor b . This yields $\phi_k = a$ for $k = 1, \dots, N/2$ and $\phi_k = b$ for $k = N/2 + 1, \dots, N$. The parameters a and b are between zero and one, $0 < a < b < 1$. Note that we do not restrict the model to $b = 1 - a$ as is often done in the literature [Feder, 1988, Peitgen *et al.*, 1992]. In the second step (generation $n = 2$), we apply the process of step 1 to the two subseries, yielding $\phi_k = a^2$ for $k = 1, \dots, N/4$, $\phi_k = ab$ for $k = N/4 + 1, \dots, N/2$, $\phi_k = ba = ab$ for $k = N/2 + 1, \dots, 3N/4$, and $\phi_k = b^2$ for $k = 3N/4 + 1, \dots, N$. In general, in step $n+1$, each subseries of step n is divided into two subseries of equal length, and the first half of the ϕ_k is multiplied by a while the second half is multiplied by b . For example, in generation $n = 3$ the values in the eight subseries are

$$a^3, a^2b, a^2b, ab^2, a^2b, ab^2, ab^2, b^3. \quad (29)$$

After n_{\max} steps, the final generation has been reached, where all subseries have length 1 and no more splitting is possible. We note that the final record can be written as

$$\phi_k = a^{n_{\max} - n(k-1)} b^{n(k-1)}, \quad (30)$$

where $n(k)$ is the number of digits 1 in the binary representation of the index k , e. g. $n(13) = 3$, since 13 corresponds to binary 1101.

For this binomial multifractal model, the formula for $\tau(q)$ has been derived earlier, see e.g. Feder [1988], Barabasi and Vicsek [1991], Peitgen *et al.* [1992], and Kantelhardt *et al.* [2002]. For convenience, we sketch the derivation in the appendix. The result is

$$\tau(q) = \frac{-\ln(a^q + b^q) + q \ln(a + b)}{\ln 2}, \quad (31)$$

$$h(q) = \frac{1}{q} - \frac{\ln(a^q + b^q)}{q \ln 2} + \frac{\ln(a + b)}{\ln 2}. \quad (32)$$

It is easy to see that $h(1) = 1$ for all values of a and b . Thus, in this form the model is limited to cases where $h(1)$, which is the exponent Hurst defined originally in the R/S method, is equal to one. In order to generalize this multifractal cascade process such that any value of $h(1)$ is possible, we have subtracted the offset $\Delta h = \ln(a + b)/\ln(2)$ from $h(q)$. The constant offset Δh corresponds to additional long-term correlations incorporated in the binomial model. For generating records without this offset, we rescale the power spectrum. First we Fast-Fourier transform (FFT) the simple binomial multifractal record (30) into the frequency domain. Then we multiply all Fourier coefficients by $f^{-\Delta h}$, where f is the frequency. This way, the slope β of the power spectra $E(f) \sim f^{-\beta}$ (the squares of the Fourier coefficients) is decreased from $\beta = 2h(2) - 1 = [2 \ln(a + b) - \ln(a^2 + b^2)]/\ln 2$ into $\beta' = [h(2) - \Delta h] - 1 = -\ln(a^2 + b^2)/\ln 2$, which is consistent with Eq. (25). Finally, backward FFT is employed to transform the signal back into the time domain. A similar Fourier filtering technique has been used by *Tessier et al.* [1996] when generating surrogate runoff data.

D. Comparison with Model Data

In order to see how well the extended binomial cascade model fits to the real data (for a given river), we generate the model data as follows: (i) we determine a and b for the given river (by best fit of Eq. (25)), (ii) we generate the simple binomial multifractal model with the obtained a and b values. (iii) We implement the proper long-term correlations as described above.

Figure 10(a) shows the DFA analysis of the model data with parameters a and b determined for the river Weser. By comparing with Fig. 5(a) we see that the extended model gives the correct scaling of the fluctuation functions $F_q(s)$ on time scales above the crossover. By comparing Fig. 10(b) with Fig. 5(c) we see that the shuffled model series becomes uncorrelated without multifractality like for the shuffled data. Below the crossover, however, the model does not yield the observed $F_q(s)$ in the original data. In the following we show that in order to obtain the proper behaviour below the crossover, either seasonal trends that cannot be completely eliminated from the data or a different type of multifractality below the crossover, represented by different values of a and b , have to be introduced.

To show the effect of seasonal trends, we have multiplied the elements ϕ_i of the extended cascade model by $0.1 + \sin^2(\pi i/365)$. Figure 10(c) shows the DFA4 result for the generalized fluctuation functions, which now better resembles the real data than Fig. 10(a). Finally, in Fig. 10(d) we show the effect of a different multifractality below the crossover, where different parameters a and b characterize this regime. The results also show better agreement with

the real data. When comparing Figs. 10(a,c,d) with Figs. 5 and 6, it seems that Danube, Amper and Wertach fit better to Fig. 10(d), i.e. suggesting different multifractality for short and large time scales, while Weser, Susquehanna and Niger fit better to Fig. 10(c) where seasonal trends are responsible for the behaviour below the crossover.

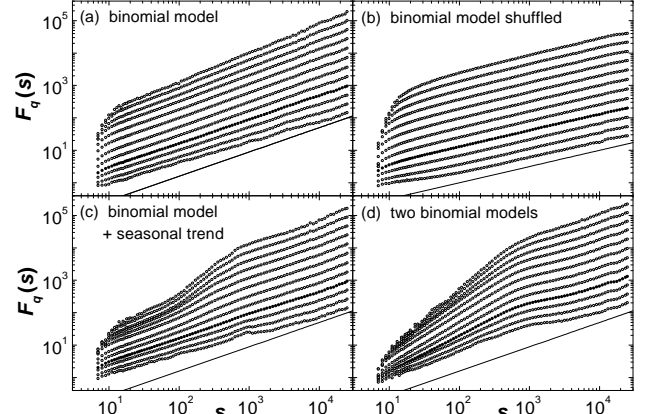


FIG. 10. The fluctuation functions $F_q(s)$ obtained from the multifractal DFA4 for surrogate series generated by the modified binomial multifractal model (see text) with parameters $a = 0.50$ and $b = 0.68$, that correspond to the values we obtained for the river Weser. The fluctuation function $F_q(s)$ for (a) the original ϕ_i series and (b) the shuffled series are plotted versus scale s for the same values of q as in the other figures. In (c) the ϕ_i have been multiplied by $0.1 + \sin^2(\pi i/365)$ before the analysis to simulate a seasonal trend. In (d) modified values of the parameters a and b ($a = 0.26$, $b = 0.59$) have been used on scales $s \leq 256$ to simulate the apparent stronger multifractality on smaller scales observed for most rivers. The straight lines in the figures have slopes $h = 0.75$ in (a,c,d) and $h = 0.5$ in (b) and are shown for comparison. For the figure, results from 10 surrogate series of length 140 years were averaged.

IV. CONCLUSION

In this study, we analyzed the scaling behaviour of daily runoff time series of 18 representative rivers in southern Germany and 23 international rivers using both, the Detrended Fluctuation Analyses (DFA) method and wavelet techniques. In all cases we found that the fluctuations exhibit self-affine scaling behaviour and long-term persistence on time scales ranging from months to decades. The fluctuation exponent H varies from river to river in a wide range between 0.55 and 0.95, showing non-universal scaling behaviour. On short time scales (below 30-100 days) the daily runoffs show a very different behaviour: They are nonstationary and characterized by H values being close to 1.5, similar to Brownian noise.

We also studied the multifractal properties of the runoff time series using a multifractal generalization of the DFA method that was crosschecked with the WTMM technique. We found that the multifractal spectra of all 41 records can be consistently described by a 'universal' function $\tau(q) = -\ln(a^q + b^q)/\ln 2$, which can be obtained from a generalization of the binomial multifractal model and has solely two

parameters a and b or, equivalently, the fluctuation exponent $H = \frac{1}{2} - \ln(a^2 + b^2)/\ln 4$ and the width $\Delta\alpha = \ln \frac{a}{b} / \ln 2$ of the singularity spectrum. Since our function for $\tau(q)$ applies also for negative q values, we could derive the singularity spectra $f(\alpha)$ from the fits. We have calculated and listed the values of H , a , b , and $\Delta\alpha$ for all records considered. There are no significant differences between their distributions for rivers in South Germany and for international rivers. We suggest that the values of H and $\Delta\alpha$ can be regarded as 'fingerprints' for each station or river, which can serve as an efficient non-trivial test bed for the state-of-the-art precipitation-runoff models. Furthermore, the generalization of the binomial multifractal model we described allows to generate and test multifractal surrogate data with specific properties for each river. We believe that such surrogate data is practically relevant for an improved flood statistics.

We have also investigated the origin of the multifractal scaling behaviour by comparison with the corresponding shuffled data. We found that the multifractality is removed by shuffling that destroys the time correlations in the series while the distribution of the runoff values is not altered. After shuffling, we obtain $h(q) \approx 1/2$ for all values of q , indicating monofractal behaviour. Hence, our results suggest that the multifractality is not due to the existence of a broad, asymmetric (singular) probability density distribution [Anderson and Meerschaert, 1998], but due to a specific dynamical arrangement of the values in the time series, i.e. a self-similar 'clustering' of time patterns of values on different time scales. We believe that our results will be useful also to improve the understanding of extreme values (singularities) in the presence of multifractal long-term correlations and trends.

V. APPENDIX: BINOMIAL MULTIFRACTAL MODEL

The binomial multifractal model series of $N = 2^{n_{\max}}$ numbers ϕ_k with $k = 1, \dots, N$ is defined by Eq. (30),

$$\phi_k = a^{n_{\max} - n(k-1)} b^{n(k-1)},$$

where $0 < a < b < 1$ are two parameters and $n(k)$ is the number of digits equal to 1 in the binary representation of the index k , e. g. $n(13) = 3$, since 13 corresponds to binary 1101.

The scaling exponents $\tau(q)$ can be calculated straightforwardly. The box probability $p_{2s}(\nu) = z_{\nu 2s} - z_{(\nu-1)2s}$ in the ν th segment of size $2s$ is given by

$$\begin{aligned} p_{2s}(\nu) &= p_s(2\nu - 1) + p_s(2\nu) \\ &= [a/b + 1]p_s(2\nu) = p_s(2\nu)(a + b)/b. \end{aligned}$$

Thus, according to Eqs. (16) and (30),

$$\begin{aligned} Z_q(s) &= \sum_{\nu=1}^{N/s} [p_s(\nu)]^q = \sum_{\nu=1}^{N/2s} [p_s(2\nu - 1)]^q + [p_s(2\nu)]^q \\ &= \left[\frac{a^q}{b^q} + 1 \right] \sum_{\nu=1}^{N/2s} [p_s(2\nu)]^q \end{aligned}$$

$$= \frac{a^q + b^q}{(a + b)^q} \sum_{\nu=1}^{N/2s} [p_{2s}(\nu)]^q = \frac{a^q + b^q}{(a + b)^q} Z_q(2s)$$

and according to Eqs. (16) and (19) we obtain the results for $h(q)$ and $\tau(q)$, Eqs. (31) and (32).

ACKNOWLEDGMENTS

We thank Diego Rybski for very useful discussions on cascade models. This work was supported by the BMBF, the DAAD, and the DFG.

- [1] Anderson, P. L. and M. M. Meerschaert, Modelling river flows with heavy tails, *Water Resources Research*, 34(9), 2271-2280, 1998.
- [2] Arneodo, A., B. Audit, N. Decoster, J.-F. Muzy, and C. Vaillant, Wavelet Based Multifractal Formalism: Applications to DNA Sequences, Satellite Images of the Cloud Structure, and Stock Market Data, in: Bunde, Kropp, and Schellnhuber [2002], pp. 27-102.
- [3] Barabasi, A., and T. Vicsek, Multifractality of self-affine fractals, *Phys. Rev. A*, 44, 2730-2733, 1991.
- [4] Bunde, A., S. Havlin, J. W. Kantelhardt, T. Penzel, J.-H. Peter, and K. Voigt, Correlated and Uncorrelated Regions in Heart-Rate Fluctuations during sleep, *Phys. Rev. Lett.*, 85(17), 3736-3739, 2000.
- [5] Bunde, A., J. Kropp, and H.-J. Schellnhuber (eds.), The science of disaster: climate disruptions, market crashes, and heart attacks, Springer, Berlin, 2002.
- [6] Feder, J., Fractals, Plenum Press, New York, 1988.
- [7] Frisch, U., and G. Parisi, Fully developed turbulence and intermittency, in: Turbulency and predictability in geophysical fluid dynamics, edited by M. Ghil, R. Benzi, and G. Parisi, North Holland, New York, 1985, pp. 84-92.
- [8] Govindan, R. B., D. Vyushin, A. Bunde, S. Brenner, S. Havlin, and H.-J. Schellnhuber, Global Climate Models Violate Scaling of the Observed Atmospheric Variability, *Phys. Rev. Lett.*, 89, 028501, 2002.
- [9] Gupta V. K. and D. R. Dawdy, Physical Interpretations of regional Variations in the scaling Exponents of Flood Quantiles, in: Kalma, J. D., Scale issues in hydrological modelling, Wiley, Chichester, 1995, pp. 106-119.
- [10] Gupta, V. K., O. J. Mesa, and D. R. Dawdy, Multiscaling theory of flood peaks: Regional quantile analysis, *Water Resources Research*, 30(12), 3405-3421, 1994.
- [11] Havlin, S., R. B. Selinger, M. Schwartz, H. E. Stanley, and A. Bunde, Random Multiplicative Processes and Transport in Structures with Correlated Spatial Disorder, *Phys. Rev. Lett.*, 61(13), 1438-1441, 1988.
- [12] Hu, K., P. Ch. Ivanov, Z. Chen, P. Carpena, and H. E. Stanley, Effect of trends on detrended fluctuation analysis, *Phys. Rev. E*, 64, 011114, 2001.

[13] Hurst, H. E., Long-term storage capacity of reservoirs, *Transactions of the American Society of Civil Engineering*, 116, 770-799, 1951.

[14] Hurst, H. E., R. P. Black, and Y. M. Simaika, Long-term storage: An experimental study, Constable & Co. Ltd., London, 1965.

[15] Kantelhardt, J. W., E. Koscielny-Bunde, H. H. A. Rego, S. Havlin, and S. Bunde, Detecting long-range correlations with detrended fluctuation analysis, *Physica A*, 295, 441-454, 2001.

[16] Kantelhardt, J. W., S. A. Zschiegner, E. Koscielny-Bunde, S. Havlin, A. Bunde, and H. E. Stanley, Multifractal detrended fluctuation analysis of nonstationary time series, *Physica A*, 316, 87-114, 2002.

[17] Koscielny-Bunde, E., A. Bunde, S. Havlin, and Y. Goldreich, Analysis of daily temperature fluctuations, *Physica A*, 231 (4), 393-396, 1996.

[18] Koscielny-Bunde, E., A. Bunde, S. Havlin, H. E. Roman, Y. Goldreich, and H.-J. Schellnhuber, Indication of a Universal Persistence Law Governing Atmospheric Variability, *Phys. Rev. Lett.*, 81(3), 729-732, 1998.

[19] Lavalée, D., S. Lovejoy, and D. Schertzer, Nonlinear variability and landscape topography: analysis and simulation, in: *Fractals in Geography. PTR Prentic-Hall*, edited by L. DeCola and N. Lam, pp. 158-192, 1993.

[20] Livina, V. N., Y. Ashkenazy, P. Braun, R. Monetti, A. Bunde, and S. Havlin, Nonlinear Volatility of River Flux Fluctuations, *Phys. Rev. E* (in press), preprint cond-mat/0209586.

[21] Lovejoy, S. and D. Schertzer, Nonlinear Variability in Geophysics: Scaling and Fractals, Kluver Academic Publ., Dordrecht, Netherlands, 1991.

[22] Mandelbrot, B. B., and J. R. Wallis, Noah, Joseph, and operational hydrology, *Water Resources Research*, 4(5), 909, 1968.

[23] Mandelbrot, B. B., and J. R. Wallis, Some long-run properties of geophysical records, *Water Resources Research*, 5(2), 321-340, 1969.

[24] Matsoukas C., S. Islam, I. Rodriguez-Iturbe, Detrended fluctuation analysis of rainfall and streamflow time series, *Journal of Geophysical Research Atmospheres*, 105(D23), 29165-29172, 2000.

[25] Menabde, M., and M. Sivapalan, Modelling of rainfall time series and extremes using bounded random cascades and Levy-stable distributions, *Water Resources Research*, 36(11), 3293-3300, 2000.

[26] Montanari, A., R. Rosso, and M. S. Taqqu, A seasonal fractional ARIMA model applied to the Nile River monthly flows at Aswan, *Water Resources Research*, 36(5), 1249-1259, 2000.

[27] Muzy, J. F., E. Bacry, and A. Arneodo, Wavelets and multifractal formalism for singular signals: Application to turbulence data, *Phys. Rev. Lett.*, 67, 3515-3518, 1991.

[28] Pandey, G., S. Lovejoy, and D. Schertzer, Multifractal analysis of daily river flows including extremes for basins of five to two million square kilometers, one day to 75 years, *Journal of Hydrology*, 208, 62-81, 1998.

[29] Peitgen, H.-O. , H. Jürgens, D. Saupe, Chaos and Fractals, Springer, New York, 1992, Appendix B.

[30] Pelletier, J. D., Analysis and modelling of the natural variability of climate, *Journal of Climate*, 10, 1331-1342, 1997.

[31] Pelletier, J. D., and D. L. Turcotte, Long-range persistence in climatological and hydrological time series: analysis, modelling and application to drought hazard assessment, *Journal of Hydrology*, 203, 198-208, 1997.

[32] Pelletier, J. D., and D. L. Turcotte, Self-affine time series: II. Applications and models, *Advances in Geophysics*, 40, 91-166, 1999.

[33] Peng, C.-K., S. V. Buldyrev, S. Havlin, M. Simons, H. E. Stanley, and A. L. Goldberger, Mosaic organization of DNA nucleotides, *Phys. Rev. E*, 49(2), 1685-1689, 1994.

[34] Peters, O., C. Hertlein, and K. Christensen, A Complexity View of Rainfall, *Phys. Rev. Lett.*, 88, 018701, 2002.

[35] Rodriguez-Iturbe, I., and A. Rinaldo, *Fractal River Basins - Change and Self-Organization*, Cambridge University Press, Cambridge, 1997.

[36] Schertzer, D., and S. Lovejoy, Physical modelling and analysis of rain and clouds by anisotropic scaling multiplicative processes, *J. Geophys. Re.*, 92, 9693, 1987.

[37] Sivapalan, M., C. Jothityangkoon, and M. Menabde, Linearity and nonlinearity of basin response as a function of scale: Discussion of alternative definitions, *Water Resour. Res.*, 38, 1012, 2002.

[38] Talkner, P., and R. O. Weber, Power spectrum and detrended fluctuation analysis: Application to daily temperatures, *Phys. Rev. E*, 62(1), 150-160, 2000.

[39] Taqqu, M. S., V. Teverovsky, and W. Willinger, Estimators for long-range dependence: An empirical study, *Fractals* 3, 785-798, 1995.

[40] Tessier Y., S. Lovejoy, P. Hubert, D. Schertzer, and S. Pecknold, Multifractal analysis and modelling of rainfall and river flows and scaling, causal transfer functions, *Journal of Geophysical Research Atmospheres*, 101(D21): 26427-26440, 1996.

[41] Turcotte, D. L. and L. Greene, A scale-invariant approach to flood-frequency analysis, *Stoch. Hydrol. Hydraul.*, 7, 33-40, 1993.

[42] Weber, R. O., and P. Talkner, Spectra and correlations of climate data from days to decades, *Journal of Geophysical Research Atmospheres*, 106(D17), 20131, 2001.